ARTICLE

Topology and immersion depth of an integral membrane protein by paramagnetic rates from dissolved oxygen

M. Sameer Al-Abdul-Wahid · Raffaello Verardi ·
Gianluigi Veglia · R. Scott Prosser

Abstract In studies of membrane proteins, knowledge of protein topology can provide useful insight into both structure and function. In this work, we present a solution NMR method for the measurement the tilt angle and average immersion depth of alpha helices in membrane proteins, from analysis of the paramagnetic relaxation rate enhancements arising from dissolved oxygen. No modification to the micelle or protein is necessary, and the topology of both transmembrane and amphipathic helices are readily determined. We apply this method to the measure the topology of a monomeric mutant of phospholamban (AFA-PLN), a 52-residue membrane protein containing both an amphipathic and a transmembrane alpha helix. In dodecylphosphocholine micelles, the amphipathic helix of AFA-PLN was found to have a tilt angle of $87° \pm 1°$ and an average immersion depth of 13.2 Å. The transmembrane helix was found to have an average immersion depth of 5.4 Å, indicating residues 41 and 42 are closest to the micelle centre. The resolution of paramagnetic relaxation rate enhancements from dissolved oxygen compares favourably to those from Ni (II), a hydrophilic paramagnetic species.

Keywords Membrane protein immersion depth · Membrane protein topology · Paramagnetic relaxation rate enhancements · Solution state NMR of membrane proteins

Abbreviations

AFA-PLN	Phospholamban mutant C36A/C41F/C46A
DOPC	1,2-dioleoyl-glycero-3-*sn*-phosphocholine
DOPE	Dioleylphosphoethanolamine
EPR	Electron paramagnetic resonance
HSQC	Heteronuclear single quantum correlation
NOE	Nuclear overhauser effect
PISEMA	Polarization inversion spin exchange at magic angle
PLN, wt-PLN	Phospholamban
PRE	Paramagnetic relaxation enhancement
RDC	Residual dipolar coupling
SDS	Sodium dodecyl sulfate
SERCA	Sarco(endo)plasmic reticulum calcium ATPase

M. S. Al-Abdul-Wahid · R. S. Prosser (✉)
Department of Chemistry, University of Toronto Mississauga,
Mississauga, ON L5L 1C6, Canada
e-mail: scott.prosser@utoronto.ca

R. Verardi · G. Veglia
Department of Chemistry, University of Minnesota,
Minneapolis, MN 55455, USA

R. Verardi · G. Veglia
Department of Biochemistry, Molecular Biology,
and Biophysics, University of Minnesota, Minneapolis,
MN 55455, USA

R. S. Prosser
Department of Biochemistry, University of Toronto,
Toronto, ON M5S 1A8, Canada

Introduction

To fully understand membrane protein function, it is helpful to combine structural information with details associated with protein topology. This includes the immersion depth and orientation of the protein in the solubilizing micelle or bilayer, and the extent of solvent exposure for each residue. Solution state NMR is well

suited to the determination of membrane immersion depth with the use of paramagnetic additives designed to give rise to depth-specific relaxation effects or chemical shift perturbations. Such additives may include spin labels anchored to lipids or detergents within a given region of the membrane or be small freely diffusing paramagnetic species, whose partitioning properties across the water membrane interface create a gradient of paramagnetic effects that correlate with depth. In this article we explore the use two freely diffusing paramagnetic species, oxygen and nickel (II), and their associated paramagnetic rate enhancements on backbone amides to obtain the immersion depth and topology of phospholamban in DPC micelles.

Phospholamban (PLN) is a 52-residue membrane protein responsible for regulating the Ca^{2+} pump in cardiac muscle cells (Maclennan and Kranias 2003). In biological membranes, PLN exists predominantly as a homopentamer in exchange with the active monomeric form (Simmerman et al. 1996). Monomeric PLN inhibits the sarco(endo)plasmic reticulum calcium ATPase (SERCA), thereby inhibiting uptake of Ca^{2+} into the cardiac sarcoplasmic reticulum (Kimura et al. 1998). In both the pentameric and monomeric states, PLN adopts a helix-turn-helix structure, composed of four dynamic domains: domain Ia (residues 1–16), a short loop (17–22), domain Ib (23–30) and domain II (31–52). The structure of pentameric PLN in oriented lipid bilayers has been characterized by a "pinwheel" model (Verardi et al. 2011; Traaseth et al. 2006), where the transmembrane helix has a tilt angle of approximately 11° with respect to the bilayer normal and the amphipathic helix is almost perpendicular to the bilayer normal.

Even in SDS micelles, a strongly denaturing/depolymerizing detergent, only 10–20% of PLN is present as monomer (Maclennan and Kranias 2003). In order to determine the topology of the active monomeric form, we employ a previously described mutant, AFA-PLN (Karim et al. 2000) in which mutation of the three cysteine residues (C36A C41F C46A) prevents formation of the pentamer. Chemical shift analysis and PISEMA (polarization inversion spin exchange at magic angle) experiments (Traaseth et al. 2007) suggest AFA-PLN and wt-PLN adopt similar structures in DOPC/DOPE bilayers, in which the amphipathic helix lies almost parallel to the bilayer surface while the transmembrane helix crosses the bilayer at an angle of 24° (AFA-PLN) (Traaseth et al. 2009) or 15° (wt-PLN) (Traaseth et al. 2007) with respect to the bilayer normal. In this study, we evaluate the topology of AFA-PLN in dodecylphosphocholine (DPC) micelles, by measuring amide proton paramagnetic rate enhancements (PREs) from dissolved oxygen and nickel acetylacetonate. The two paramagnetic species have opposite partitioning properties across water membrane interfaces such that the measurement of rate enhancements from both species provides

reliable information on both solvent exposure and immersion depth.

Background

A number of approaches may be employed to study membrane protein topology by NMR. Intermolecular Nuclear Overhauser Effects (NOEs), which involve a through-space transfer of spin magnetization between ^1H spins on detergent molecules and the peptide (Losonczi et al. 2000) may identify residues which contact the micelle, although the accuracy of such NOE-based experiments suffers from spin-diffusion along the detergent/lipid acyl chain(s), as well as the dynamics of the bilayer/micelle (Huster et al. 1999). Similarly, relaxation effects from covalently anchored paramagnetic species such as nitroxide spin labels fixed to specific sites on lipids or detergents, provides a long-range measure of immersion depth. (Altenbach et al. 1994) NOEs from water to protons on membrane proteins (Dalvit and Hommel 1995a, b) may reveal water-exposed regions of the peptide. While there is a gradient in H_2O solubility across the "headgroup" region, local H_2O concentration is effectively zero throughout the hydrophobic centre (Marrink and Berendsen 1994; Marrink and Berendsen 1996). As a consequence, NOEs from water are effective at distinguishing between protein residues near the headgroup and those in the bulk water, but the NOE from water to residues located anywhere in the hydrophobic core would be zero, irrespective of the actual immersion depth. Thus, the water NOE experiment cannot provide a direct measure of the depth-dependence of residues located in the hydrophobic region of micelles/bilayers.

The relative orientation of alpha helices in a protein, and their orientation relative to the solubilising lipid environment may be obtained by measurement of $^1H–^{15}N$ residual dipolar couplings (Bax and Grishaev 2005; Tjandra and Bax 1997), which require the membrane protein to be weakly aligned via strain-induced alignment in a gel (Chou et al. 2001). Alternatively, solid state NMR measurements of proteins/lipid preparations on glass supports provide another powerful tool for determining helical orientation of membrane proteins, namely by the PISEMA experiments of Opella et al. (Wu et al. 1994). However, while both methods provide orientational information, neither measures immersion depth explicitly, instead providing information on possible tilt angles of alpha helices.

Electron paramagnetic resonance (EPR) or fluorescence experiments have provided reliable measures of structure (Altenbach et al. 1990), immersion depth (Altenbach et al. 1994), and dynamics (Steinhoff et al. 1994, 1995) of large transmembrane proteins via site-directed spin labelling.

The advantage of NMR measurements here is twofold. First, the mutagenesis and introduction of a reporter molecule (i.e. an ESR spin probe or fluorescent chromophore) necessary for most systems may introduce a local perturbation in the peptide or bilayer, whereas the only "perturbation" in NMR is the isotopic substitution of nitrogen-14 with nitrogen-15. Second, the ESR/fluorescence experiment provides the immersion depth of the reporter molecule only, necessitating multiple mutants to determine the full immersion depth profile of a protein (Altenbach et al. 1994). In contrast, NMR-based immersion depth measurements can yield the immersion depth of all resolvable amide protons simultaneously, in just one experiment requiring only one sample. If further resolution is desired, NMR-derived side-chain immersion depths may be readily obtained from samples where carbon-12 has been substituted with carbon-13. For large membrane proteins (e.g. G-protein-coupled receptors), spectral crowding and slow molecular tumbling may complicate interpretation of NMR spectra. In such cases, selectively labelling only certain residues with nitrogen-15 or carbon-13 (Rosen et al. 1996) ameliorates spectral interpretation. In cases where it is difficult or undesirable to produce isotopically labelled protein, researchers adapt techniques from ESR/fluorescence spectroscopy to introduce, minimally perturbing probe molecules, even as small as a single ^{19}F atom, to provide well-resolved NMR resonances (Bokoch et al. 2010; Kitevski-Leblanc et al. 2009).

O$_2$ as a paramagnetic reporter of immersion depth

Dissolved oxygen, which possesses two unpaired electrons, has been shown to be a very sensitive paramagnetic additive in studies of positioning and topology in model membrane systems (Altenbach et al. 1994; Al-Abdul-Wahid et al. 2006, 2009; Prosser et al. 2000). As with other paramagnetic compounds, oxygen induces chemical shift changes and paramagnetic relaxation rate enhancements (PREs) of nearby NMR spins. Chemical shift changes are easily detected on nuclei possessing a large chemical shift dispersion, such as ^{13}C or ^{19}F (Al-Abdul-Wahid et al. 2006), while PREs are better observed on nuclei with high gyromagnetic ratios, such as ^{1}H (Al-Abdul-Wahid et al. 2009) or ^{19}F. Induced paramagnetic shifts and PREs turn out to be surprisingly simple to interpret; in both cases, the magnitude of the effect scales linearly with local O$_2$ concentration, while variations in the O$_2$ diffusion rate do not significantly influence NMR-observed paramagnetic effects (Al-Abdul-Wahid et al. 2006). In contrast, site-directed spin labelling EPR experiments rely on the O$_2$ solubility-diffusion product, and may require multiple samples to fully characterize positioning and topology (Altenbach et al. 1994).

In general, the observed PRE from dissolved O$_2$ may be expressed as (Al-Abdul-Wahid et al. 2006):

$$\text{PRE}_i = j \int \rho_i(z) \times [\text{O}_2(z)]dz \tag{1}$$

where $\rho_i(z)$ is the immersion depth distribution function for residue i, and j is a global scaling factor, in units of Hz (mol/L)$^{-1}$. For the rigid amide protons of structured alpha helices, we assume that the widths of the $\rho_i(z)$ are narrow and we consider each amide proton to have an average immersion depth z_i. In this case, the PRE is simplified to:

$$\text{PRE}_i = j \times [\text{O}_2(z_i)] \tag{2}$$

As a consequence of the inherent disorder in the acyl chains of micelle-bound detergent molecules (Marrink and Berendsen 1996), oxygen is entropically driven to partition into the hydrophobic core of micelles (Al-Abdul-Wahid et al. 2011). The O$_2$ concentration gradient across a lipid bilayer may be approximated using a Boltzmann sigmoid; the same equation may be used to model the O$_2$ concentration gradient through the centre of a micelle (Marsh 2001):

$$[\text{O}_2(z)] = \left([\text{O}_2]^{\text{water}} - [\text{O}_2]^{\text{max}}\right)$$
$$\times \left(\frac{1}{1 + e^{\left(\frac{z-z_0}{\lambda}\right)}} - \frac{1}{1 + e^{\left(\frac{z+z_0}{\lambda}\right)}}\right) + [\text{O}_2]^{\text{water}} \tag{3}$$

where z is the distance from the micelle centre. In the Boltzmann sigmoid model, oxygen concentrations range from a minimum, $[\text{O}_2]^{\text{water}}$, in bulk water ($|z| > 28$ Å) to a maximum, $[\text{O}_2]^{\text{max}}$, in the hydrophobic micelle center ($z = 0$ Å). z_0 designates an immersion depth where the oxygen gradient is greatest, while λ characterizes the effective width of the distribution function. At a partial pressure of 30 bar, the $[\text{O}_2]$ gradient spans a factor of 7–10 from the bulk water interface to the centre of a lipid bilayer (Al-Abdul-Wahid et al. 2006, 2011). We exploit this gradient of $[\text{O}_2(z)]$ to measure the immersion depth profile of a membrane peptide, by measuring PREs on all resolvable amide protons in one experiment.

Ni^{2+} as a paramagnetic reporter of water exposure

Prior studies have employed hydrophilic paramagnetic additives, typically metal chelates, to probe membrane peptide topology (Su et al. 2008; Madl et al. 2009; Zangger et al. 2009; Respondek et al. 2007) and amphiphile immersion depth (Al-Abdul-Wahid et al. 2009). The concentration of hydrophilic additives scales with local [H$_2$O]. In contrast with O$_2$, water and ionic molecules are virtually

excluded from the micelle interior. Hydrophilic additives are therefore excellent reporters of water exposure, but poor at discriminating differences in the immersion depth of sites inside the hydrophobic region of micelles or bilayers. In this study, we employ nickel (II) acetylacetonate as a reporter of water exposure, and thus expect large Ni-PREs for water-exposed residues, while Ni-PREs of close to zero are expected for residues associated with the interior of transmembrane helices. A further advantage of measuring Ni-PREs in conjunction with O_2-PREs is the facile identification of tightly packed regions of the protein. Tightly packed regions would be expected to exclude both Ni^{2+} and O_2, giving rise to low PREs from both compounds. Residues exhibiting low Ni-PREs and low O_2-PREs should therefore be excluded from any determination of immersion depth or topology, as the associated PRE values do not reflect the relevant concentration gradient for a bilayer/micelle.

PRE measurements and method

The paramagnetic rate enhancement is defined as:

$$PRE = R_1^{para} - R_1^{dia} \qquad (4)$$

where R_1^{para} is the spin–lattice relaxation rate in the presence of dissolved oxygen or Ni^{2+}, and R_1^{dia} is the relaxation rate in the absence of paramagnetic additive. While PREs may be measured directly on ^1H nuclei, we choose to instead measure relaxation rates of the so-called "$H_Z N_Z$" state, a mixed quantum state of magnetization from both ^1H and the directly bound ^{15}N. Compared to direct measurement on ^1H nuclei (i.e. via HSQC), measurement of the $H_Z N_Z$ state (Kay et al. 1992; Boyd et al. 1990) is preferable due to the elimination of artifacts introduced by exchange of amide protons with those from water, and easier suppression of signals arising from H_2O. Moreover, the lower gyromagnetic ratio of the ^{15}N nucleus results in stronger PREs on the $H_Z N_Z$ state as compared to the N_Z state (Abragam 1961). In measuring proton relaxation rates in macromolecules, one must be conscious of the effects of spin diffusion (via proton-proton dipolar couplings), which tend to average or 'blur' the observed R_1 values across adjacent protons. Teng et al. (2006) note that effects of spin diffusion are strongest for protons embedded in the hydrophobic core of a protein, where dipolar couplings are more numerous, while surface protons are less affected. They also recommend measuring R_2 instead of R_1, as the shorter decay times used in the R_2 measurement reduces spin diffusion. As AFA-PLN does not have a hydrophobic core, we treat all residues are surface residues, free of the spin diffusion present in a typical hydrophobic core. In

membrane proteins, we must also consider the possibility of spin diffusion arising from dipolar couplings between detergent molecules and protein. Such couplings occur on the same timescale as R_1^{dia}. On the other hand, PREs are dominated by the R_1^{para} term; since this term is typically on the same timescale as R_1^{dia}, our measurements are effectively in the timescale suggested by Teng et al. and spin diffusion is curtailed. Thus, the lack of hydrophobic core in AFA-PLN, combined with the shorter timescale of relaxation rate measurements, limits spin diffusion sufficiently to allow residue-by-residue resolution of local paramagnet concentration.

Paramagnetic rate enhancements for alpha helices

As previously mentioned, the observed PRE for a given residue, i, is proportional to the local oxygen concentration, $[O_2](z_i)$, where we approximate $[O_2](z)$ using the previously described Boltzmann sigmoid (Teng et al. 2006). From the O_2-PREs, we extract the tilt angle with respect to the micelle/bilayer normal, θ, and average immersion depth, z_{avg}, by employing the parametric equations for an alpha helix to generate an expression for z_i that is a function of i, z_{avg}, and θ. We first consider the simple case of a transmembrane alpha helix parallel to the bilayer normal ($\theta = 0°$), in which the "rise" of the helix is 1.51 Å per residue (Pauling et al. 1951), and the z_i are described by the following:

$$z_i^{transmembrane} = 1.51 \times (i - i_{avg}) + z_{avg} \qquad (5)$$

where i_{avg} is simply the average residue number of the helix being studied and need not correspond to the centre of the bilayer (e.g. for a helix corresponding to residues 23 through 52 in the primary sequence, $i_{avg} = 37.5$). For the second obvious case, an amphipathic alpha helix ($\theta = 90°$), the z_i oscillate about z_{avg} and are described by:

$$z_i^{amphipathic} = 1.5 \times \cos\left(\frac{2\pi}{3.6}i - \varphi\right) + z_{avg} \qquad (6)$$

where the factor of 1.5 represents the inner "radius" of the alpha helix (determined empirically from analysis of PDB coordinates of alpha helices), the factor of 3.6 accounts for the periodicity of the helix (Pauling et al. 1951), φ is a phase value ranging between zero and 2π, and here z_{avg} is specifically nonzero. By combining (5) and (6), we obtain the general equation describing the z_i for any un-curved alpha helix:

$$z_i = \sin\theta\left[1.5 \times \cos\left(\frac{2\pi}{3.6}i - \varphi\right)\right] + \cos\theta[1.51 \times (i - i_{mid})] + z_{avg} \qquad (7)$$

which is analogous to the equation obtained by Zangger and co-workers for amphipathic helices (Respondek et al.

2007). From this equation for z_i and previously defined equations for the PRE (2) and $[O_2(z)]$ (3), we derive the following expression for the PRE:

$$PRE_i = j \times \left[\left([O_2]^{water} - [O_2]^{max}\right) \right.$$
$$\left. \times \left(\frac{1}{1 + e^{\left(\frac{z_i - z_0}{\lambda}\right)}} - \frac{1}{1 + e^{\left(\frac{z_i + z_0}{\lambda}\right)}} \right) + [O_2]^{water} \right] \quad (8)$$

By substituting previously measured values for $[O_2]^{max}$, $[O_2]^{water}$, z_0, and λ (Al-Abdul-Wahid et al. 2011), only four adjustable parameters remain in (8): a global scaling factor j, helix tilt angle θ, average immersion depth z_{avg}, and the phase factor φ. The values of these four parameters may then be determined by a global non-linear least squares fit of the observed PRE values to (8).

To illustrate the sensitivity of O_2-PREs as a probe of membrane protein topology, we have rotated and translated the coordinates of an alpha helix (domain II from AFA-PLN, PDB: 1N7L) to generate four alpha helices with known tilt angles and average immersion depths. O_2-PRE values for each of these helices (Fig. 1, black circles) were then predicted using the $[O_2(z)]$ of (3). We then fit each set of PRE values to (8) (Fig. 1, red lines) to extract a tilt angle and immersion depth. The resulting fits demonstrate that O_2-PREs easily discriminate small ($\sim 10°$) differences in the tilt angle of amphipathic helices (Fig. 1, panels c, d), but may struggle in discriminating modest ($\sim 30°$) differences in the tilt angle of transmembrane helices. We now apply this technique to extract helical tilt angle and immersion depth from the experimentally observed O_2-PREs of the amphipathic and transmembrane helices of monomeric phospholamban.

Results and discussion

As a small membrane protein, AFA-PLN provides sharp, well-resolved resonances (Fig. 2) and good (86%) assignment of $H_Z N_Z$ spectra is achieved at moderate Larmor frequencies (e.g. 600 MHz). R_1 values are then extracted from a fit of the peak intensities as a function of the magnetization recovery time; the PRE is then calculated as the difference in R_1 in the presence and absence of the relevant paramagnetic species. Figure 3 shows measured peak intensities and the fitted relaxation decay curves for S16 and L44. Paramagnetic broadening from 30 bar O_2 increases line widths by an average of only ~ 4 Hz and does not affect assignment. O_2-PREs (Fig. 4, upper panel) span a factor of 6, from ~ 3 Hz for residues in the loop region and domain Ib to ~ 14.5 Hz for residues near the centre of domain II. In a separate experiment, Ni-PREs (Fig. 4, lower panel) were determined to range from 0 to 19 Hz, although strong paramagnetic broadening results in
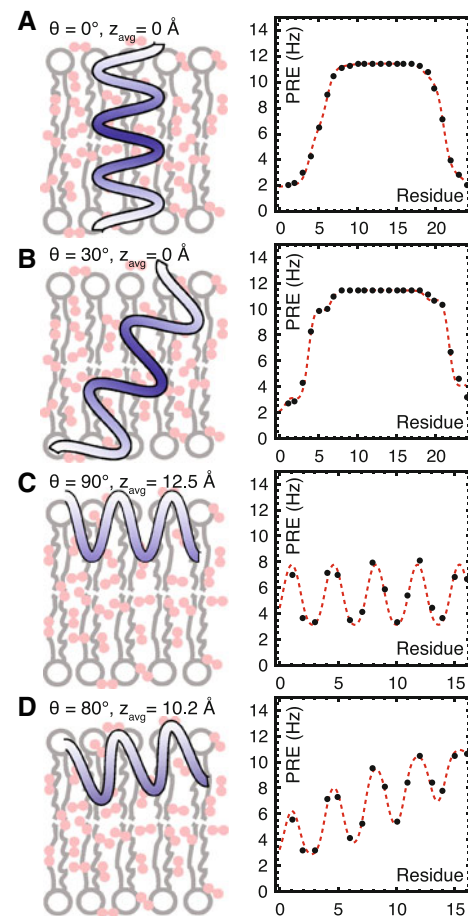

Fig. 1 Four possible scenarios for an uncurved alpha helix in a membrane protein, along with predicted amide proton O_2-PRE values (*black circles*) and corresponding fits to (8) (*dashed red lines*). The PDB co-ordinates for residues 30–52 of AFA-PLN (PDB: 1N7L) were rotated by 0°, 30°, 90°, and 80°, for scenarios **a** through **d**, respectively, and then translated by 12.5 and 10.5 Å for scenarios **c** and **d**. O_2-PRE values were then predicted by inputting these coordinates into (2). The tilt angle and average immersion depth were then determined by a non-linear least squares fit of the predicted PRE values to (8), as described in the text. The fitted tilt angles for scenarios **a** through **d**, are 4.17°, 29.5°, 90.0°, and 79.4°, respectively, while the fitted average immersion depths are 12.64 and 10.38 Å for *panels* **c** and **d**. For each scenario, a cartoon on the *left side* provides a pictorial representation of the alpha helix in a membrane, and is not drawn to scale. Due to space considerations, only the first 16 residues are graphed in *panels* **c** and **d**

assignment of only 63% of amide backbone residues in the presence of Ni^{2+}. In some cases, residues expected to have a high degree of water exposure (as determined via low O_2-PREs, and as suggested by other models of AFA-PLN), such as N-terminal residues 2 and 3, water-exposed loop residue 22, C-terminal residue 52, are completely broadened away. In other cases (e.g. various residues in domain Ia and II), moderate line broadening results in loss of assignment due to peak overlap. In particular, the negatively charged carboxylate anions of Glu-2, Glu-19, and the
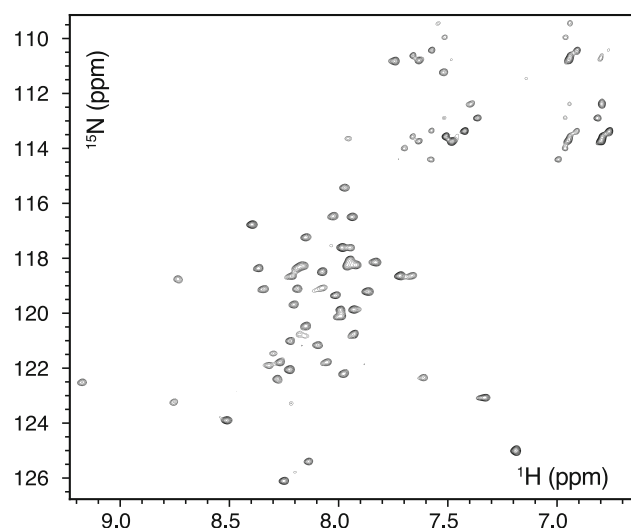
Fig. 2 Representative [^{1}H, ^{15}N] TROSY-enhanced H$_Z$N$_Z$ spectrum of AFA-PLN in DPC micelles, at 37°C, in the presence of 30 bar dissolved O$_2$. The magnetization recovery delay was 4 ms
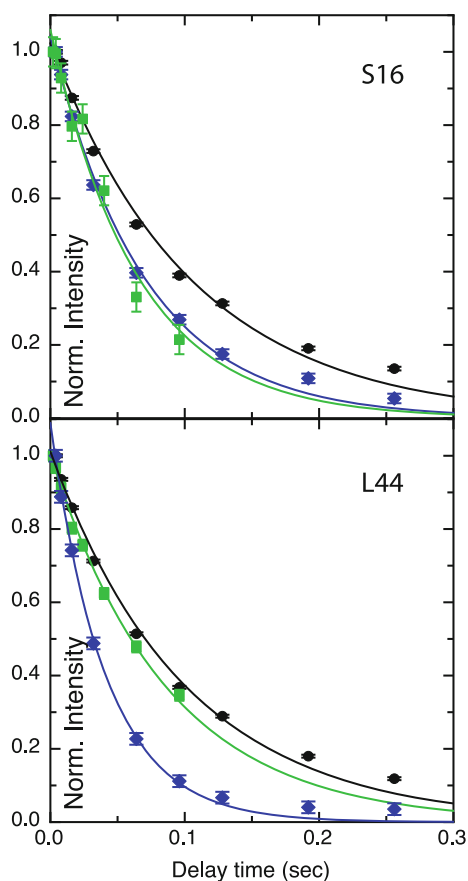

Fig. 3 Experimental peak intensities and fitted relaxation decay curves for S16 (*top panel*) and L44 (*bottom panel*) in the absence of paramagnetic compounds (*black circles and line*), in the presence of 30 bar O$_2$ (*blue diamonds and line*), and in the presence of 1 mg/mL Ni(acac)$_2$ (*green squares and line*). Peak intensities have been normalized to unity for the shortest delay time, and have been fitted to exponential decay functions of the form $Le^{K(-x)}$
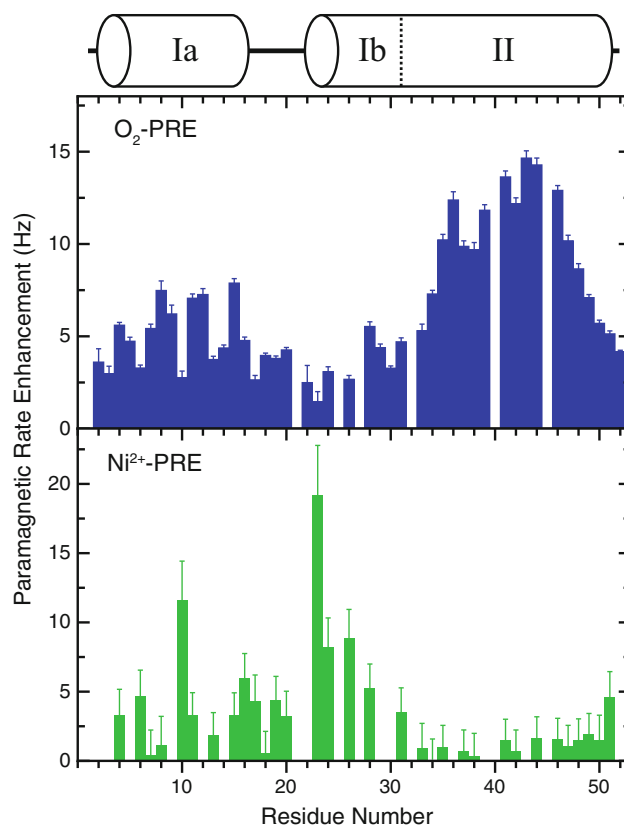

Fig. 4 Paramagnetic rate enhancements of backbone amide protons of AFA-PLN in DPC micelles, arising from 30 bar dissolved O$_2$ (*blue bars*) and 1 mg/mL Ni(acac)$_2$ (*green bars*). The secondary structure of AFA-PLN is overlaid on *top* for reference

C-terminal Leu-52 may serve as electrostatic binding partners for Ni^{2+}. None of the residues in AFA-PLN exhibit both low Ni-PRE and low O$_2$-PRE values, suggesting the absence of any tightly packed regions that may confound the determination of helical tilt angles and immersion depths.

In order to extract topological information from O$_2$-PREs, we must first select appropriate values for the non-adjustable parameters in the Boltzmann sigmoid [O$_2(z)$]. [O$_2$]^{water} is calculated to be 26.8 mM at an O$_2$ partial pressure of 30 bar and a temperature of 37°C (Weiss [1970]). We employ [O$_2$]^{max} = 161 mM, z_0 = 11.73 Å, λ = 1.26, as determined in previous work on lipid bilayers (Al-Abdul-Wahid et al. [2011]). Although the above parameters are not specifically for a spherical micelle, we make the assumption that the coating of DPC molecules around AFA-PLN will conform to the hydrophobic regions of the protein, and the resulting aggregate will not be spherical.

Domain Ia (residues 1–16)

Domain Ia exhibits moderate O$_2$-PREs and Ni-PREs, indicating contact with both the micelle and bulk water.

Moreover, there is a clear oscillation in O_2-PREs as a function of residue number (Fig. 5, upper panel) suggesting the helical axis is not parallel to the O_2 concentration gradient. Indeed, the alpha helix comprising domain Ia is amphipathic (Fig. 6). Residues on the apolar face exhibit an average O_2-PRE of 6.5 Hz compared to an average of 3.6 Hz for those on the polar face, indicating the apolar face is more buried in the micelle and therefore faces the micelle centre. This is consistent with a previous Gd^{3+}-based paramagnetic study of wt-PLN that determined three residues on the apolar face were oriented towards the centre of the lipid bilayer (Traaseth et al. 2007), and a recent model of AFA-PLN in which the apolar face is also oriented towards the bilayer center (Shi et al. 2011). From a non-linear least squares fit of the observed O_2-PREs to (8)
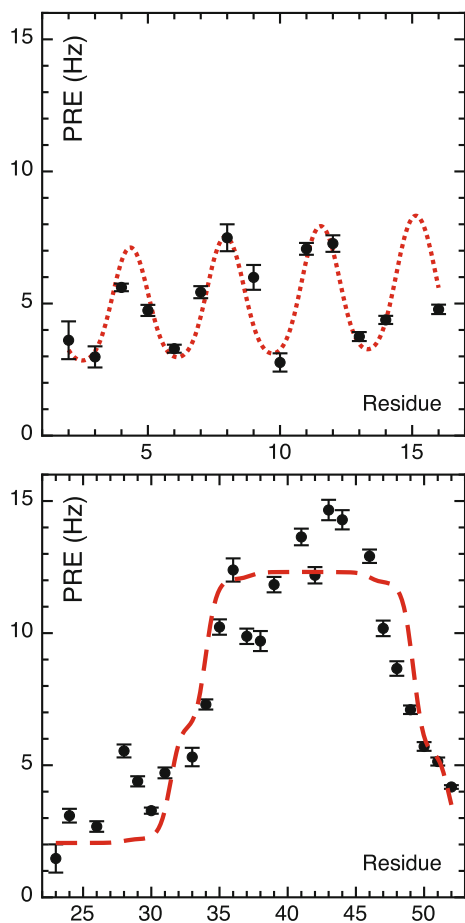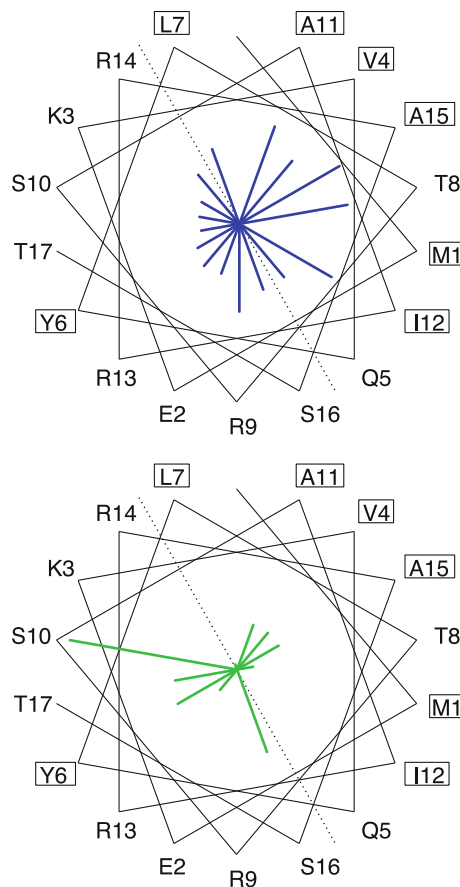

Fig. 6 Helical wheel representations of Helix I of AFA-PLN, with PREs arising from 30 bar dissolved O_2 shown as *blue rays* (*top*) and PREs arising from 1 mg/mL Ni^{2+} shown as *green rays* (*bottom*). *Boxes* around the residue label indicate hydrophobic residues, while the *dotted line* represents the theoretical division between the hydrophobic and hydrophilic faces of the helix

Fig. 5 Paramagnetic rate enhancements arising from 30 bar dissolved O_2 (*black circles*) for the amphipathic helix (*top panel*) and the transmembrane helix (*bottom panel*) of AFA-PLN. Non-linear least squares regressions of the PRE values to (8) are shown as *red lines*. For the amphipathic helix, the average immersion depth is 13.2 Å with a tilt angle of $87° \pm 1°$. For the transmembrane helix, residues 41 and 42 are in the centre of the micelle (i.e. $z_{avg} = 5.4$ Å), and the helix would be expected to adopt a tilt angle of $25° \pm 4°$ in DMPC bilayers

(Fig. 5, upper panel), we report the tilt angle relative to the bilayer normal as $87° \pm 1°$, and the average immersion depth as 13.2 ± 0.3 Å. As previously discussed, the Boltzmann sigmoid $[O_2]$ used in this fit is derived from a DMPC-like bilayer; in such bilayers, 13.5 Å is the average immersion depth of the carbonyl groups on the acyl chain (Al-Abdul-Wahid et al. 2006). Previous measures of tilt angle range from 92° to 93° from solid state NMR studies of wt-PLN (Traaseth et al. 2007) and AFA-PLN (Traaseth et al. 2006) to 102° from an NMR-based MD simulation of AFA-PLN in DOPC bilayers (Traaseth et al. 2009). The same MD simulation also reported an average immersion depth of 16.2 ± 0.8 Å for the amphipathic helix in DOPC bilayers; in these bilayers, the average immersion depth of the carbonyl groups is 16.3 Å. We therefore conclude that domain Ia adopts a tilt angle of $87° \pm 1°$ in DPC micelles, and that the helix favours the carbonyl region of lipid bilayers. We also note there is no sinusoidal pattern to Ni-PRE values; Ni^{2+} does not provide the same spatial degree

of resolution as O_2. This is due in part to the loss of assignment of 6 residues from paramagnetic line broadening, and may also be a consequence of steric considerations; the Ni^{2+} complex ion cannot sample the protein backbone as well as the smaller O_2 molecule. In either event, the practical utility of O_2-PREs is unmatched.

Domains Ib (residues 23–30) and II (residues 31–52)

Low O_2-PREs and high Ni-PREs suggest domain Ib is in significant contact with the bulk water, in agreement with recent models of AFA-PLN (Traaseth et al. 2009; Shi et al. 2011; Zamoon et al. 2008). Of particular interest is Glu-23, which has the distinction of both the lowest O_2-PRE *and* highest measured Ni-PRE, suggesting a high degree of water exposure; in fact an MD simulation of AFA-PLN (Traaseth et al. 2009) suggests Glu-23 is the most water-exposed residue in the protein. Domain II comprises a transmembrane helix, and both O_2-PRE and Ni-PRE values reflect the polarity gradient of detergent micelles. Residues 41–44 exhibit the largest O_2-PREs observed in AFA-PLN and represent the putative centre of the transmembrane helix, while low Ni-PREs (<1.9 Hz) for the region between residues 31 and 51 confirms that Domain II is in a water-free environment (i.e. the micelle interior). The ends of the transmembrane region are marked by low O_2-PREs for residues 31 and 52 and moderate Ni-PREs (i.e. >3.5 Hz) at residues 31, 51, and 52, suggesting moderate contact with water for these residues. A fit of O_2-PREs for the entire helix (i.e. domains Ib and II) to (8) (Fig. 5, lower panel) calculates the tilt angle relative to the bilayer normal as $25° \pm 4°$, and the average immersion depth as 5.4 ± 0.5 Å. The larger error in tilt angle, as compared to domain Ia, is a result of the insensitivity of this fitting method in determining the tilt angle of transmembrane helices. However, the calculated tilt angle is sensible given the length of the helix, and agrees with recent studies reporting the tilt angle to be between 21° and 28°, depending on the solubilising detergent (Traaseth et al. 2009; Arkin et al. 1995; Smith et al. 2001). Furthermore, the calculated average immersion depth places residues 41 and 42 at the centre of the micelle, and is in excellent agreement with a recent MD simulation of AFA-PLN in DOPC bilayers (Traaseth et al. 2009), which reported an average immersion depth of 5.5 ± 0.5 Å for the helix comprising domains Ib and II.

Conclusions

We have demonstrated a minimally perturbing method of measuring the tilt angle and immersion depth of the alpha helices of membrane proteins, which utilizes the natural O_2 solubility gradient present in micelles and bilayers. Compared to other methods, our NMR-based technique is advantageous in that the O_2-PREs of all amide protons are measured in a single experiment, obviating the need for mutagenesis or multiple samples. Similarly, Ni-PREs provide a complementary assessment of water exposure, which when combined with O_2-PREs, distinguish immersion depth from solvent exposure. The only requirements in performing these measurements are that the protein be ^{15}N-labelled and the N–H spectrum be previously assigned (or assignable from a ^{13}C, ^{15}N-labelled sample of the protein). Knowledge of secondary structural elements is helpful but not required, as O_2-PREs readily identify transmembrane and amphipathic helices. In AFA-PLN, O_2-PREs span a factor of 6 across the micelle and clearly identify the transmembrane and amphipathic helices. A global nonlinear least squares fit of O_2-PREs to an alpha helical model reports the amphipathic helix adopts a tilt angle of $87° \pm 1°$ with respect to the micelle normal, and would be located near the carbonyl groups of a DMPC bilayer, while the transmembrane helix is expected to adopt a tilt angle of $25° \pm 4°$ in DMPC bilayers, with residues Phe-41 and Leu-42 closest to the hydrophobic centre. At a partial O_2 pressure of 30 bar, O_2-PREs are readily observed for all assignable residues, providing Angstrom-level resolution of the immersion depth profile of AFA-PLN. In contrast, Ni-PREs suffer from paramagnetic broadening for certain water-exposed residues, and the near-zero solubility of Ni^{2+} in the hydrophobic region of the micelle results in a lack of lack of depth-dependant information for residues located therein. Furthermore, the smaller molecular radius of O_2 allows it to sample smaller void volumes in a peptide/micelle complex, which a relatively bulky Ni^{2+} complex ion would not be able to access. The charge associated with Ni^{2+} may further confound measurements, as residence times of the Ni^{2+} ion in the vicinity of negatively charged residues or the micelle headgroups may result in Ni-PREs that are not representative of local water exposure. In such cases, the use of different chelating groups around the central metal ion may reduce binding to charge groups on the protein (Pintacuda and Otting 2002). Although data from side-chain protons were not necessary in determining the topology of AFA-PLN, in more complex systems O_2-PREs from side-chain surface protons may be used to refine membrane protein topology. Finally, experiments using dissolved O_2 are straightforward to implement at the partial pressures needed to obtain sensitive spatial resolution; samples are easily recovered via degassing, whereas the removal of hydrophilic additives requires dialysis or similar purification techniques.

In this work, the O_2 distribution in the micelle was modeled using a Boltzmann sigmoid, with the relevant parameters ($[O_2]^{max}$, z_0, and λ) obtained from a previous

study of $[O_2]$ in lipid bilayers (Al-Abdul-Wahid et al. 2011). The validity of utilizing these parameters to study AFA-PLN in detergent micelles may be assessed by simultaneously varying $[O_2]^{max}$, z_0, and λ, to $\pm 20\%$ of their original value and determining the change in the calculated the tilt angles and immersion depths of the helices of AFA-PLN. Across this range of $[O_2]^{max}$, z_0, and λ, the tilt angle of the amphipathic helix spans less than $\pm 0.7°$, while the average immersion depth varies by ± 2.3 Å. Conversely, for the transmembrane helix, the calculated tilt angle varies by a considerable $\pm 16°$, while the average immersion depth spans ± 0.7 Å. In essence, measurements of the tilt angle of amphipathic helices and the immersion depth of transmembrane helices are robust, while systematic errors in the calculated immersion depth of amphipathic helices and the tilt angle of transmembrane helices may arise from incorrect values of $[O_2]^{max}$, z_0, or λ.

Helical tilt angles and immersion depths obtained from O_2-PREs may aid in membrane protein structural determination. In particular, residual dipolar couplings (RDCs) provide orientational information (Tjandra and Bax 1997), which may be used for structure refinement (Clore et al. 1998; Tjandra et al. 2000). However, the RDC equation contains 16-fold degeneracy (Hus et al. 2008), and while this may be reduced to fourfold degeneracy under certain circumstances (Jensen and Blackledge 2008), analysis of RDCs remains complicated by these so-called 'ghost orientations'. Bertini and co-workers recently demonstrated the use of paramagnetic-based restraints to eliminate ghost orientations (Bertini et al. 2007), and a similar method was recently applied to lift RDC degeneracy in an NMR-derived structure of AFA-PLN (Shi et al. 2011). For alpha helices, measurement of tilt angles via O_2-PREs should allow facile elimination of ghost orientations from the analytical solutions of the RDC equation. Meanwhile, average immersion depths extracted from O_2-PREs may aid in determining the overall positioning of the membrane protein in the bilayer.

Materials and methods

Uniformly-labeled ^{15}N AFA-PLN was prepared as previously described (Buck et al. 2003), to a final concentration of ~ 0.8 mM in a 300 mM DPC, 25 mM phosphate, pH 7 buffer for NMR analysis. Nickel acetylacetonate was used as obtained from Sigma Chemicals (Mississauga, ON). All NMR experiments were performed on a 600 MHz Varian Inova spectrometer and either a triple resonance cold probe or room temperature probe, at a sample temperature of 310 K. A previously described TROSY-enhanced H_ZN_Z experiment (Evanics et al. 2006) was used to measure R_1 values, using a series of nine values ranging from 2 to

256 ms for the magnetization recovery delay. Typical spectra were acquired with 16 scans and 128 increments, spanning 2,000 Hz in the indirect dimension. PREs from O_2 and Ni^{2+} were obtained by subtracting the H_ZN_Z spin–lattice relaxation rates in the absence of any paramagnetic additive from the rate obtained under a partial O_2 pressure of 30 bar or with the addition of 1 mg/mL nickel acetyl-acetonate. O_2 measurements were performed in a 5 mm sapphire NMR tube (Saphikon, NH). Samples were pre-equilibrated at an O_2 partial pressure of 30 bar for at least 2 days prior to measuring relaxation rates to ensure a constant $[O_2]$ during the experiments. Spectra were processed with the NMRPIPE processing suite (Delaglio et al. 1995). FID signals consisting of 1,802 complex points in the direct dimension were zero filled to 4,096 points along with squared-cosine apodization before Fourier transformation. In the indirect dimension, FID signals consisting of 256 points were linear predicted to 512 points, zero filled to 2,048 points and processed with squared-cosine apodization before Fourier transformation. R_1 values and errors were obtained using NMRViewJ (Johnson and Blevins 1994); the signal-to-noise in each spectrum was used as the standard deviation for the Monte Carlo procedure built into NMRViewJ. Non-linear least squares fits of experimental PRE values to (8) were performed using the "Nonlinear-ModelFit" routine in Mathematica. This routine provides an option to incorporate the experimental error in each observed PRE in determining the best parameters to the fit; reported errors for tilt angles and immersion depths are therefore based on both the experimental error and the fitting error.

References

Abragam A (1961) The principles of nuclear magnetism. Clarendon Press, Oxford

Al-Abdul-Wahid MS, Yu C-H, Batruch I, Evanics F, Pomes R, Prosser RS (2006) A combined NMR and molecular dynamics study of the transmembrane solubility and diffusion rate profile of dioxygen in lipid bilayers. Biochemistry 45:10719–10728

Al-Abdul-Wahid MS, Neale C, Pomes R, Prosser RS (2009) A solution NMR approach to the measurement of amphiphile immersion depth and orientation in membrane model systems. J Am Chem Soc 131:6452–6459

Al-Abdul-Wahid MS, Evanics F, Prosser RS (2011) Dioxygen transmembrane distributions and partitioning thermodynamics in lipid bilayers and micelles. Biochemistry 50:3975–3983

Altenbach C, Marti T, Khorana H, Hubbell W (1990) Transmembrane protein-structure—spin labeling of bacteriorhodopsin mutants. Science 248:1088–1092

J Biomol NMR (2011) 51:173–183

Altenbach C, Greenhalgh DA, Khorana HG, Hubbell WL (1994) A collision gradient method to determine the immersion depth of nitroxides in lipid bilayers: application to spin-labeled mutants of bacteriorhodopsin. Proc Natl Acad Sci USA 91:1667–1671

Arkin I, Rothman M, Ludlam C, Aimoto S, Engelman D, Rothschild K, Smith S (1995) Structural model of the phospholamban ion-channel complex in phospholipid-membranes. J Mol Biol 248:824–834

Bax A, Grishaev A (2005) Weak alignment NMR: a hawk-eyed view of biomolecular structure. Curr Opin Struct Biol 15:563–570

Bertini I, Gupta YK, Luchinat C, Parigi G, Peana M, Sgheri L, Yuan J (2007) Paramagnetism-based NMR restraints provide maximum allowed probabilities for the different conformations of partially independent protein domains. J Am Chem Soc 129:12786–12794

Bokoch MP, Zou Y, Rasmussen SGF, Liu CW, Nygaard R, Rosenbaum DM, Fung JJ, Choi H-J, Thian FS, Kobilka TS, Puglisi JD, Weis WI, Pardo L, Prosser RS, Mueller L, Kobilka BK (2010) Ligand-specific regulation of the extracellular surface of a G-protein-coupled receptor. Nature 463:108–112

Boyd J, Hommel U, Campbell ID (1990) Influence of cross-correlation between dipolar and anisotropic chemical-shift relaxation mechanisms upon longitudinal relaxation rates of N-15 in macromolecules. Chem Phys Lett 175:477–482

Buck B, Zamoon J, Kirby TL, DeSilva TM, Karim C, Thomas D, Veglia G (2003) Overexpression, purification, and characterization of recombinant Ca-ATPase regulators for high-resolution solution and solid-state NMR studies. Protein Expr Purif 30:253–261

Chou J, Gaemers S, Howder B, Louis J, Bax A (2001) A simple apparatus for generating stretched polyacrylamide gels, yielding uniform alignment of proteins and detergent micelles. J Biomol NMR 21:377–382

Clore GM, Gronenborn AM, Tjandra N (1998) Direct structure refinement against residual dipolar couplings in the presence of rhombicity of unknown magnitude. J Magn Reson 131:159–162

Dalvit C, Hommel U (1995a) Sensitivity-improved detection of protein hydration and its extension to the assignment of fast-exchanging resonances. J Magn Reson B 109:334–338

Dalvit C, Hommel U (1995b) New pulsed-field gradient NMR experiments for the detection of bound water in proteins. J Biomol NMR 5:306–310

Delaglio F, Grzesiek S, Vuister GW, Zhu G, Pfeifer J, Bax A (1995) NMRpipe—a multidimensional spectral processing system based on unix pipes. J Biomol NMR 6:277–293

Evanics F, Hwang PM, Cheng Y, Kay LE, Prosser RS (2006) Topology of an outer-membrane enzyme: measuring oxygen and water contacts in solution NMR studies of PagP. J Am Chem Soc 128:8256–8264

Hus JC, Salmon L, Bouvignies G, Lotze J, Blackledge M, Brüschweiler R (2008) 16-Fold degeneracy of peptide plane orientations from residual dipolar couplings: analytical treatment and implications for protein structure determination. J Am Chem Soc 130:15927–15937

Huster D, Arnold K, Gawrisch K (1999) Investigation of lipid organization in biological membranes by two-dimensional nuclear overhauser enhancement spectroscopy. J Phys Chem B 103:243–251

Jensen MR, Blackledge M (2008) On the origin of NMR dipolar waves in transient helical elements of partially folded proteins. J Am Chem Soc 130:11266–11267

Johnson BA, Blevins RA (1994) NMR view—a computer-program for the visualization and analysis of NMR data. J Biomol NMR 4:603–614

Karim CB, Marquardt CG, Stamm JD, Barany G, Thomas DD (2000) Synthetic null-cysteine phospholamban analogue and the corresponding transmembrane domain inhibit the Ca-ATPase. Biochemistry 39:10892–10897

Kay LE, Nicholson LK, Delaglio F, Bax A, Torchia DA (1992) Pulse sequences for removal of the effects of cross-correlation between dipolar and chemical-shift anisotropy relaxation mechanism on the measurement of heteronuclear T1 and T2 values in proteins. J Magn Reson 97:359–375

Kimura Y, Asahi M, Kurzydlowski K, Tada M, MacLennan D (1998) Phospholamban domain Ib mutations influence functional interactions with the Ca2+-ATPase isoform of cardiac sarcoplasmic reticulum. J Biol Chem 273:14238–14241

Kitevski-Leblanc JL, Evanics F, Prosser RS (2009) Approaches for the measurement of solvent exposure in proteins by F-19 NMR. J Biomol NMR 45:255–264

Losonczi J, Olejniczak E, Betz S, Harlan J, Mack J, Fesik S (2000) NMR studies of the anti-apoptotic protein Bcl-x(L) in micelles. Biochemistry 39:11024–11033

Maclennan DH, Kranias EG (2003) Calcium: phospholamban: a crucial regulator of cardiac contractility. Nat Rev Mol Cell Biol 4:566–577

Madl T, Bermel W, Zangger K (2009) Use of relaxation enhancements in a paramagnetic environment for the structure determination of proteins using NMR spectroscopy. Angew Chem Int Ed 48:8259–8262

Marrink S, Berendsen H (1994) Simulation of water transport through a lipid-membrane. J Phys Chem Us 98:4155–4168

Marrink S, Berendsen H (1996) Permeation process of small molecules across lipid membranes studied by molecular dynamics simulations. J Phys Chem Us 100:16729–16738

Marsh D (2001) Polarity and permeation profiles in lipid membranes. Proc Natl Acad Sci USA 98:7777–7782

Pauling L, Corey RB, Branson HR (1951) The structure of proteins—2 hydrogen-bonded helical configurations of the polypeptide chain. Proc Natl Acad Sci USA 37:205–211

Pintacuda G, Otting G (2002) Identification of protein surfaces by NMR measurements with a paramagnetic Gd(III) chelate. J Am Chem Soc 124:372–373

Prosser RS, Luchette PA, Westerman PW (2000) Using O_2 to probe membrane immersion depth by 19F NMR. Proc Natl Acad Sci USA 97:9967–9971

Respondek M, Madl T, Goebl C, Golser R, Zangger K (2007) Mapping the orientation of helices in micelle-bound peptides by paramagnetic relaxation waves. J Am Chem Soc 129:5228–5234

Rosen M, Gardner K, Willis R, Parris W, Pawson T, Kay L (1996) Selective methyl group protonation of perdeuterated proteins. J Mol Biol 263:627–636

Shi L, Traaseth NJ, Verardi R, Gustavsson M, Gao J, Veglia G (2011) Paramagnetic-based NMR restraints lift residual dipolar coupling degeneracy in multidomain detergent-solubilized membrane proteins. J Am Chem Soc 133:2232–2241

Simmerman H, Kobayashi Y, Autry J, Jones L (1996) A leucine zipper stabilizes the pentameric membrane domain of phospholamban and forms a coiled-coil pore structure. J Biol Chem 271:5941–5946

Smith S, Kawakami T, Liu W, Ziliox M, AIMOTO S (2001) Helical structure of phospholamban in membrane bilayers. J Mol Biol 313:1139–1148

Steinhoff H, Mollaaghababa R, Altenbach C, Hideg K, Krebs M, Khorana H, Hubbell W (1994) Time-resolved detection of structural-changes during the photocycle of spin-labeled bacteriorhodopsin. Science 266:105–107

Steinhoff H, Mollaaghababa R, Altenbach C, Khorana H, Hubbell W (1995) Site-directed spin-labeling studies of structure and dynamics in bacteriorhodopsin. Biophys Chem 56:89–94

Su Y, Mani R, Hong M (2008) Asymmetric insertion of membrane proteins in lipid bilayers by solid-state NMR paramagnetic relaxation enhancement: a cell-penetrating peptide example. J Am Chem Soc 130:8856–8864

Teng C, Hinderliter B, Bryant R (2006) Oxygen accessibility to ribonuclease A: quantitative interpretation of nuclear spin relaxation induced by a freely diffusing paramagnet. J Phys Chem A 110:580–588

Tjandra N, Bax A (1997) Direct measurement of distances and angles in biomolecules by NMR in a dilute liquid crystalline medium. Science 278:1111–1114

Tjandra N, Marquardt J, Clore GM (2000) Direct refinement against proton-proton dipolar couplings in NMR Structure determination of macromolecules. J Magn Reson 142:393–396

Traaseth NJ, Buffy JJ, Zamoon J, Veglia G (2006) Structural dynamics and topology of phospholamban in oriented lipid bilayers using multidimensional solid-state NMR. Biochemistry 45:13827–13834

Traaseth NJ, Verardi R, Torgersen KD, Karim CB, Thomas DD, Veglia G (2007) Spectroscopic validation of the pentameric structure of phospholamban. Proc Natl Acad Sci USA 104:14676–14681

Traaseth NJ, Shi L, Verardi R, Mullen DG, Barany G, Veglia G (2009) Structure and topology of monomeric phospholamban in lipid membranes determined by a hybrid solution and solid-state NMR approach. Proc Natl Acad Sci 106:10165

Verardi R, Shi L, Traaseth NJ, Walsh N, Veglia G (2011) Structural topology of phospholamban pentamer in lipid bilayers by a hybrid solution and solid-state NMR method. Proc Natl Acad Sci USA 108:9101–9106

Weiss R (1970) Solubility of nitrogen, oxygen and argon in water and seawater. Deep Sea Res 17:721–735

Wu CH, Ramamoorthy A, Opella SJ (1994) High-resolution heteronuclear dipolar solid-state NMR-spectroscopy. J Magn Reson Ser A 109:270–272

Zamoon J, Mascioni A, Thomas DD, Veglia G (2008) NMR solution structure and topological orientation of monomeric phospholamban in dodecylphosphocholine micelles. Biophys J 85:2589–2598

Zangger K, Respondek M, Goebl C, Hohlweg W, Rasmussen K, Grampp G, Madl T (2009) Positioning of micelle-bound peptides by paramagnetic relaxation enhancements. J Phys Chem B 113:4400–4406